Vol. 14 • No. 11 • March 20 • 2026

www.advopticalmat.de

ADVANCED OPTICAL MATERIALS

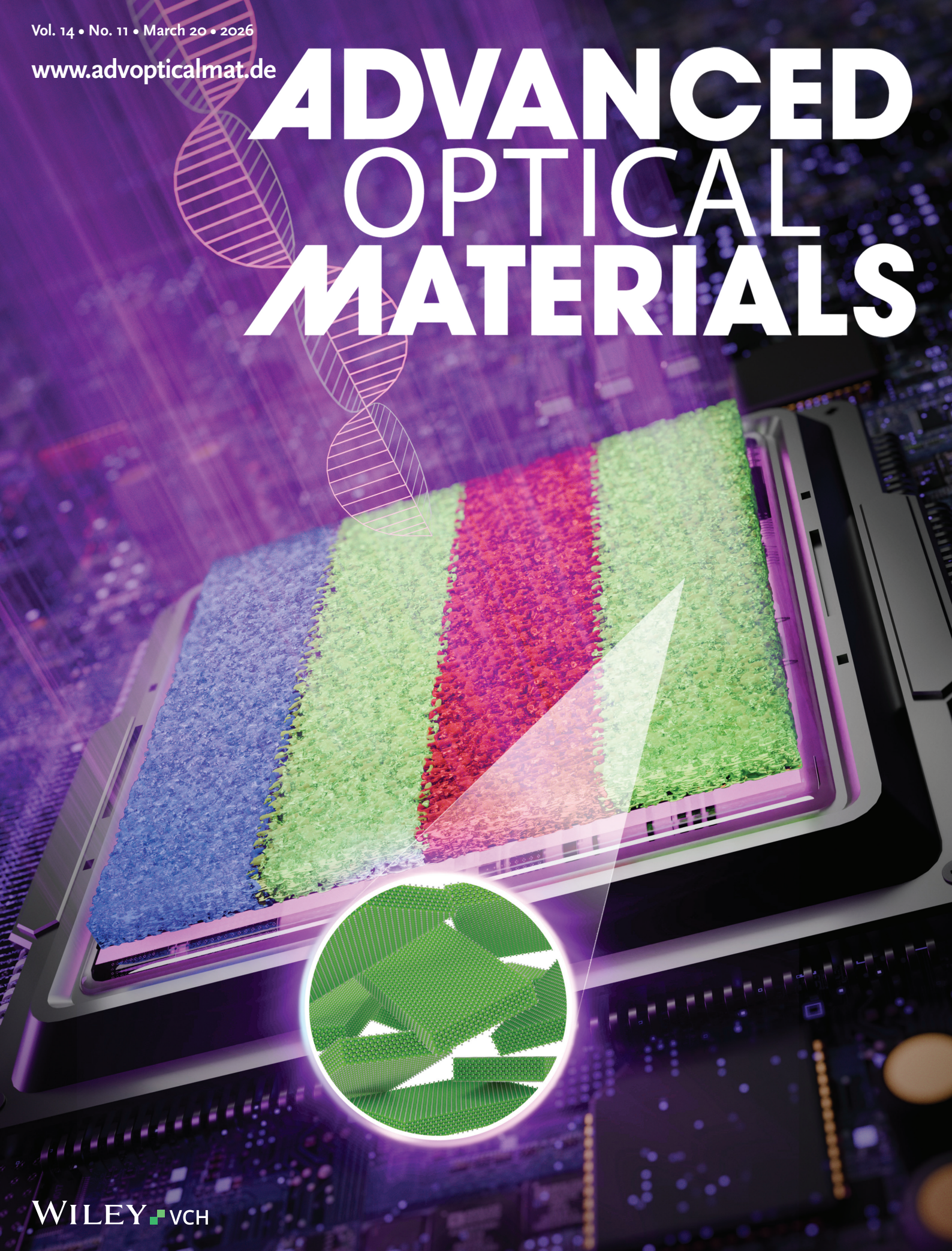

WILEY VCH

RESEARCH ARTICLE

ADVANCED OPTICAL MATERIALS
www.advopticalmat.de

Ultra-Durable Information-Encoded Anti-Counterfeiting Self-Assembled Nanocrystal Labels

*Taha Haddadifam, Farzan Shabani, Mustafa Kalay, Aisan Khaligh, Evren Mutlugun, Mustafa Serdar Onses, and Hilmi Volkan Demir**

Forgery, a serious universal problem, is causing huge economic losses every year. Against forgery, information-encoded labelling systems have attracted significant attention for a diverse range of anti-counterfeiting applications. Here, cost-effective and ultra-durable nanocrystal-based labels are proposed and demonstrated in which information can be encoded as physically unclonable functions (PUFs) of hardware-oriented security systems. The fabrication method of the PUFs is based on the self-assembly of colloidal quantum wells (CQWs) and generation of unclonable features within their pattern at a liquid–liquid interface. These CQW PUFs are analyzed with well-known statistical tests, which show a uniqueness level of 0.5060 ± 0.0323 and prove their randomness. In addition, a feature-matching algorithm is used to authenticate these information-encoded CQW PUFs. For the safety of the semiconductor chips, a CQW PUF is attached to the surface of the chip to protect against hardware cyber-attacks. Eventually, fabricated labels are examined against high temperatures and moisture environments. The fabricated CQW label is durable for a period of 150 days it is tested, demonstrating ultra-high stability of the label. High stability and durability, cost-effectiveness, and high encoding capacity make these proposed nanocrystal labels extremely attractive for large-scale commercialization.

1. Introduction

Today, counterfeiting is a globally critical issue, impacting both the world economy and human health. It was estimated by Frontier Economics that the worldwide economic loss due to forgery is in the range of several trillion US dollars annually.[1] There is an urgent strong need to develop cost-effective technologies for reliable anti-counterfeiting label manufacturing.[2–4] With the swift expansion of the Internet of Things (IoT) devices, the security of the electronics and the integrated circuits is crucial.[5] Today, software-based verification systems are widespread. However, they are vulnerable to cyber-attacks. Therefore, the advancement of hardware-oriented validation mechanisms is essential for recognizing counterfeit devices.[6] Numerous structures have previously been reported in anti-counterfeiting applications, including surface-enhanced Raman scattering (SERS) structures,[7] holograms,[8]

T. Haddadifam, F. Shabani, A. Khaligh, H. V. Demir
UNAM—Institute of Materials Science and Nanotechnology
The National Nanotechnology Research Center
Department of Electrical and Electronics Engineering
Department of Physics
Bilkent University
Bilkent, Ankara, Turkey
E-mail: volkan@bilkent.edu.tr

M. Kalay
Department of Electricity and Energy
Kayseri University
Kayseri, Turkey

E. Mutlugun
Department of Electrical-Electronics Engineering
Abdullah Gül University
Kayseri, Turkey

M. S. Onses
ERNAM–Erciyes University Nanotechnology Application and Research Center
Department of Materials Science and Engineering
Erciyes University
Kayseri, Turkey

H. V. Demir
Luminous! Center of Excellence for Semiconductor Lighting and Displays
School of Electrical and Electronic Engineering
Division of Physics and Applied Physics
School of Physical and Mathematical Sciences
School of Materials Science and Engineering
Nanyang Technological University
Singapore 639798, Singapore

The ORCID identification number(s) for the author(s) of this article can be found under https://doi.org/10.1002/adom.202502884

DOI: 10.1002/adom.202502884

molecular tags, graphical barcodes,[9] and fluorescent labels.[10–16] Nevertheless, these structures typically suffer from combinations of some major limitations, including complex encryption, limited encoding capacity, demand for special equipment, and high fabrication costs.[7] On the other hand, physically unclonable functions (PUFs) are in high demand to be resistant to physical attacks while being cost-effective and are required to provide high encoding capacity at the same time.[7] PUFs utilize randomness generated by the fabrication process to produce unique and secure keys. Therefore, duplicating these PUFs is impossible thanks to their fingerprint-like nature. Optical, arbiter and memory-based structures have been previously used as PUFs.[17,18]

Various materials have been investigated in the fabrication of such anti-counterfeiting labels, including lanthanide-doped inorganic nanomaterials,[19] organic dyes,[20] semiconductor quantum dots,[21,22] perovskites,[23] and plasmonic nanomaterials.[24,25] Nonetheless, despite their favorable physically unclonable functionality, some of these materials face specific disadvantages inherent in their material properties, restricting their utilization in anti-counterfeiting labels. In the case of plasmonic PUFs, the fabrication of 2D security labels from plasmonic materials requires expensive techniques such as electron beam lithography.[3] Since the creation of these labels is costly, their large-scale use is limited for industrial applications. For example, organic dyes could undergo photobleaching after a certain time.[26] Furthermore, perovskites suffer from stability issues.[27] To fabricate high-performance labels with real-world applicability, materials should ideally provide critical features including narrow emission bandwidth, straightforward synthesis, high quantum yield, photobleaching resistance, and low-cost synthesis. Quantum dots have been recognized as a promising candidate to be used for hardware security in anticounterfeiting applications, thanks to their tunable and size-dependent optical properties.[28] The solution-based synthesis of the colloidal quantum dots (CQDs) offers a vast variety of compositions, sizes and heterostructures which can be realized by cost-effective methods.[29] The information-encoded labels based on solution-processed materials like CQDs have been explored. However, CQDs could not provide an ultra-narrow emission bandwidth feature due to the inhomogeneous size variation of the nanoparticles limiting their encoding capacity.[30] On the other hand, colloidal quantum wells (CQWs), known for their ultra-narrow emission, could possibly address this issue. However, no PUFs of CQWs have been reported to date.

Several methods have been reported for fabricating anti-counterfeiting cloneable and unclonable labels capable of encoding information. Among them are printing,[31] writing, lithography, electrospraying,[13] and assisted assembly.[32] Printing techniques such as ink-jet printing and screen-printing methods are widely used for the preparation of security labels.[3,32] While these well-known printing methods offer great features like high resolution, they suffer from minor issues like the coffee ring effect.[33] Lithography is known for its high stability and precision,[34] but it is a costly method, resulting in the fabrication of expensive labels. In the assisted assembly approach, nanoparticles are initially self-assembled on a surface, and then, with the aid of a template, this thin film turns into a pattern by removing the extra nanoparticles.[25] However, the mass production of these templates is costly since a new template should be designed and fabricated for every size and pattern. A combination of the mentioned fabrication methods has also been employed. For instance, by using lithography and self-assembly, SERS substrates can be fabricated.[35] Low-cost, high-speed, and large-scale fabrication of unclonable labels are important factors required in anti-counterfeiting label manufacturing.

Here, we designed and fabricated PUF labels of multi-color CQWs that allow for information to be encoded in high capacity, either spatially, spectrally, or both (opto-spatially). Using their self-assembly[36] at the liquid-liquid interface, it is possible to fabricate various junctions, including metal-semiconductor, metal-dielectric, and semiconductor-dielectric as stripe patterns in a thin film. Our method is simple to operate, rapid and cost-effective, and requires no special equipment. Such quasi-2D CQWs possibly offer the ultra-narrow emission bandwidth thanks to their atomically flat surface and suppression of inhomogeneous broadening.[37] In this work, CQWs were used in PUF labels owing to their unique properties such as controllable thickness at atomic accuracy, ultra-narrow emission bandwidth, and large absorption cross-section.[37–41] In spectral encoding, achieving high encoding capacity requires extremely narrow emission to produce spectrally distinguishable and observable colors. To the best of our knowledge, this is the first demonstration of spectral and spatial information encoding fabricated through a novel yet simple approach and using state-of-the-art CQWs. To be considered as PUFs, we generated randomness in the boundaries of the stripes by using an excessive amount of silicone oil. This encoding of information, combined with PUFs, makes the information inimitable since inherent randomness makes the label replication unachievable. Statistical tests were carried out to check the randomness level of the labels. Also, authentication of the labels was achieved using feature feature-matching algorithm. To transfer labels onto the target, tattoo papers[42] were used to separate the fabrication process from the target object and transfer an information-encoded label onto the surface of a chip. We conducted stability tests to examine the stability and durability of the CQW labels. We showed the stability of the PUF label against heating and humidity, and its durability over 150 days. **Figure 1** shows the schematic diagram of the proposed approach.

2. Results and Discussion

Throughout this work, miscellaneous CdSe-based CQWs with high color purity and ultra-narrow emission bandwidths, including blue-emitting $CdSe_{0.7}S_{0.3}$/CdS core/crown, green-emitting CdSe/CdS core/crown, red-emitting CdSe/CdZnS core/shell, and orange-emitting CdSe/ZnS core/shell CQWs, were synthesized to be used in anticounterfeiting labelling. These CQWs possess the best properties both for providing ultra-narrow tunable emission and the ability to control their self-assembly. **Figure 2** exhibits the absorption and emission spectra, and the transmission electron microscopy (TEM) images of the blue-, green-, orange-, and red-emitting CQWs, correspondingly. All the CQWs possess typical absorption profiles of quasi-2D CQWs with distinguishable electron-light hole and electron-heavy hole excitonic peaks at lower photon energies.[43] For the blue- and green-emitting CQWs, as the crown was grown laterally around

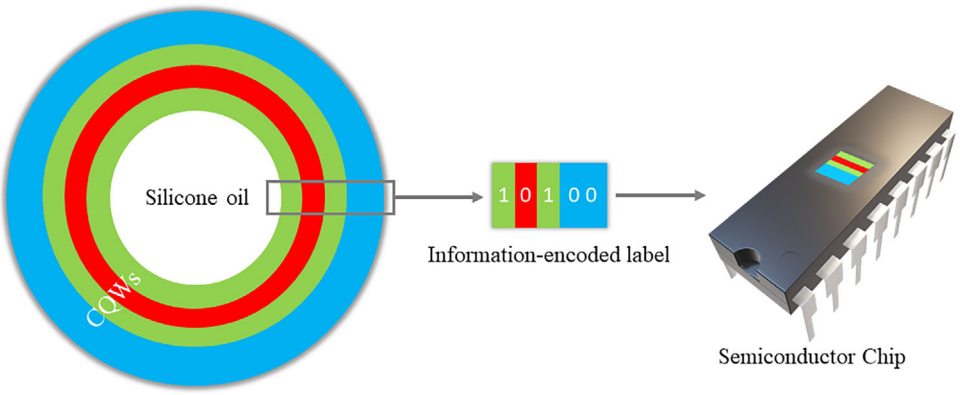

Figure 1. A schematic diagram of the labelling process.

the CdSe or CdSeS core, a third peak associated with this domain emerges,[44] while for the orange and red CQWs with a shell, the absorption profile red-shifts due to the relaxed quantum confinement with no new peaks.[45] The TEM images further confirm the 2D shape of the grown CQWs with different lateral shapes due to the different synthesis mechanisms of these CQWs.

The X-ray diffraction (XRD) patterns of the CQWs in Figure S1 (Supporting Information) show that all the CQWs possess a zinc blende crystalline structure with trivial differences in the diffracted peak positions (Table S1, Supporting Information) due to the distinct compositions and domains.[46] Moreover, the survey and resolved X-ray photoelectron spectroscopy (XPS) spectra of these CQWs in Figures S2–S5 (Supporting Information) demonstrate the participation of the elements in the preferred state with no sign of Se oxidation.[37] Time-resolved fluorescence (TRF) decay curves of the CQWs in Figure S6 (Supporting Information) show that the core/shell CQWs with relaxed confinement possess longer lifetimes as a consequence of the large distance between the electron and hole, as expected.[37,47] TRF decay components are given in Table S2 (Supporting Information).

2.1. Colloidal Nanoparticle Patterning

We utilized a bi-phase assembly method in which colloidal nanoparticles can be patterned in an ordered manner to fabricate self-assembled labels. Hexane was chosen as the solvent for its optimal evaporation rate and high dispersibility of CQWs, which facilitates large self-assembled film fabrication with a smooth surface.[48] Furthermore, diethylene glycol was used as the po-

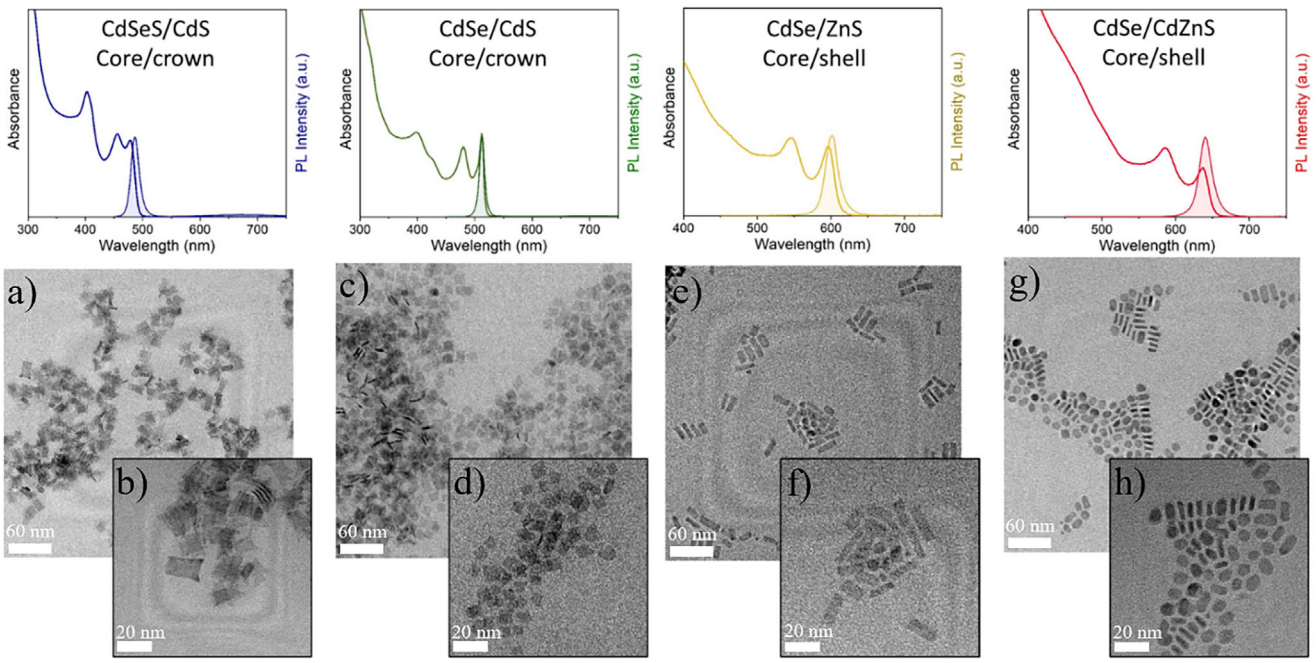

Figure 2. Absorption and photoluminescence (PL) spectra (first row) and TEM images (second row) of the synthesized CQWs: a,b) blue $CdSe_{0.7}S_{0.3}$/CdS core/crown CQWs, c,d) green CdSe/CdS core/crown CQWs, e,f) yellow CdSe/ZnS core/shell CQWs, and g,h) red CdSe/CdZnS core/shell CQWs.

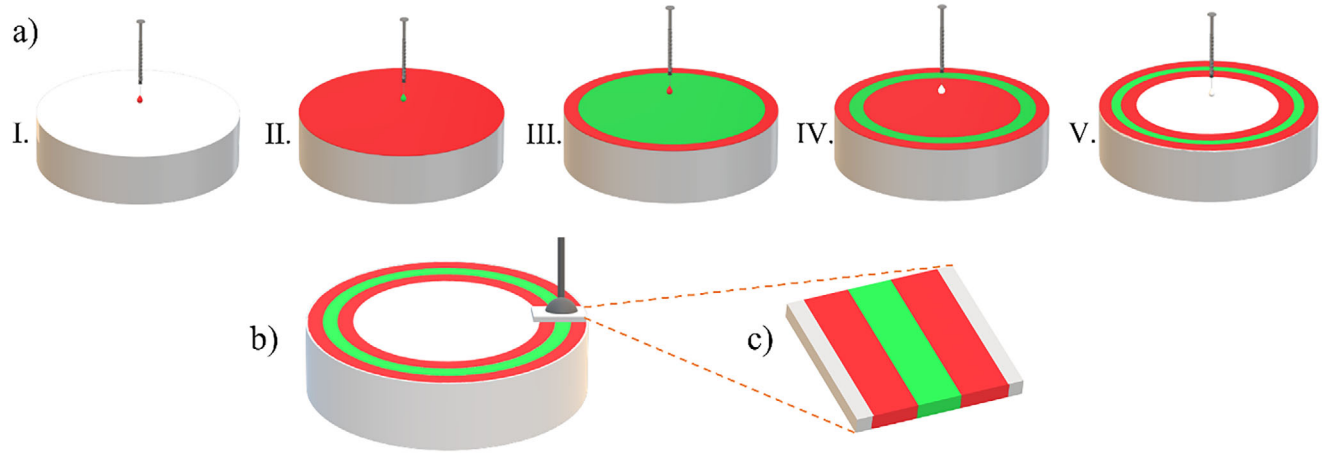

Figure 3. a) Process flow of ring-like pattern generation procedure. I. The first macrodroplet containing red CQWs falls on the subphase in the center of the Petri dish. II. The second macrodroplet of green CQWs. III. The third macrodroplet of red CQWs. IV. Silicone oil macrodroplet falls for pushing the rings. V. The Second macrodroplet of silicone oil pushes the rings further to achieve the desired ring width. b) Schematic of transferring the pattern to the substrate using the stamping technique. c) Illustration of the transferred pattern on the substrate with three stripes after subphase evaporation.

lar subphase for its ideal viscosity to inhibit the mixing of the two phases. CQWs are self-assembled on the diethylene glycol in a controlled manner to form a specific pattern. The patterning system is shown in Figure S13 (Supporting Information).

Figure 3a depicts a step-by-step schematic of our patterning procedure. Herein, a syringe was used to instill one macrodroplet of the host CQWs with high concentration from the center of the Petri dish filled with the subphase liquid (Figure 3a-I). This macrodroplet was used to make a certain margin from the edge of the Petri dish. Patterning is initiated by dropping a controlled sequence of macrodroplets on the subphase, resulting in a ring-like pattern (Figure 3a-II,III). The newly instilled CQWs do not blend with previously dropped CQWs due to the agglomeration and conceivably different surface chemistry, which enables well-defined pattern formation. The interfacial energy model provides a good description of the underlying physics behind this phenomenon. Herein, the CQWs tend to minimize their total surface free energy through agglomeration, which decreases the exposed surface area. The underlying mechanisms and dynamics are further detailed in the Supporting Information (Figure S25, Supporting Information). In addition, each ring is composed of densely packed CQWs, without any gap with other rings, making a well-connected junction. After the pattern was formed, silicone oil was used to compress the rings and make a ring-like pattern near the edge of the Petri dish (Figure 3a-IV). We used a certain concentration of the silicone oil to diminish the ring width to the desired size (Figure 3a-V). Since the width of the rings is much lower than the diameter of the Petri dish, these rings are considered as stripes in a small area with no curvature. Due to the extreme concentration of the host material, the height of the host stripe and the other stripes are different (Figure S12, Supporting Information). The pattern can be transferred onto the substrate using the stamping technique, as shown in Figure 3b. Eventually, the substrate needs to be put under vacuum to evaporate the remaining subphase or other volatile species. Figure 3c displays the schematic of the final pattern on the substrate with three stripes.

To gain a thorough understanding of the patterning procedure, a model was developed (Supporting Information). Herein, the width and height of the rings depend on diverse parameters such as concentration of the CQWs, amount of injected silicone oil, macrodroplet formation time, and petri dish diameter. Using a 90 mm-diameter Petri dish, and an approximate macrodroplet formation time of one second, the width of the stripes can be finely tuned by CQW concentration in solution and the number of macrodroplets. The concentration of the silicone oil should be optimized to push the CQWs to the narrowest possible ring width. As an alternative approach, increasing the number of macrodroplets can also compress the rings. Using different concentrations of silicone oil, we can control the ring width in the pattern. Employing the same material concentrations, macrodroplet volume, and silicone oil concentration results in a negligible error in the ring width across separate experiments, indicating reproducibility of the ring formation. The minimized difference between the patterns is likely from the rapid hexane evaporation, resulting in material concentration variation.

This substantial control over the pattern formation proved to be extremely critical for spatial, spectral, and opto-spatial encoding, which will be explained in the following section.

2.2. Spatial Encoding

Adopting our patterning method, we can fabricate labels in which the information is encoded spatially. In the spatial encoding, the arrangement of the rings is vital. Every stripe is one bit of data, which is defined as 1 or 0 in binary format. For instance, the American Standard Code for Information Interchange (ASCII) for the word "Bilkent" is "0 100 0010 0 110 1001 0 110 1100 0 110 1011 0 110 0101 0 110 1110 0 111 0100". For encoding this word and generating its label, 56 stripes are required, with red-emitting stripes representing 1, with another color (blue, green, or other) stripes representing 0. **Figure** 4a shows the corresponding data for this word. As discussed earlier, the stripes demonstrate high quality in terms of defectless self-assembly, which is of

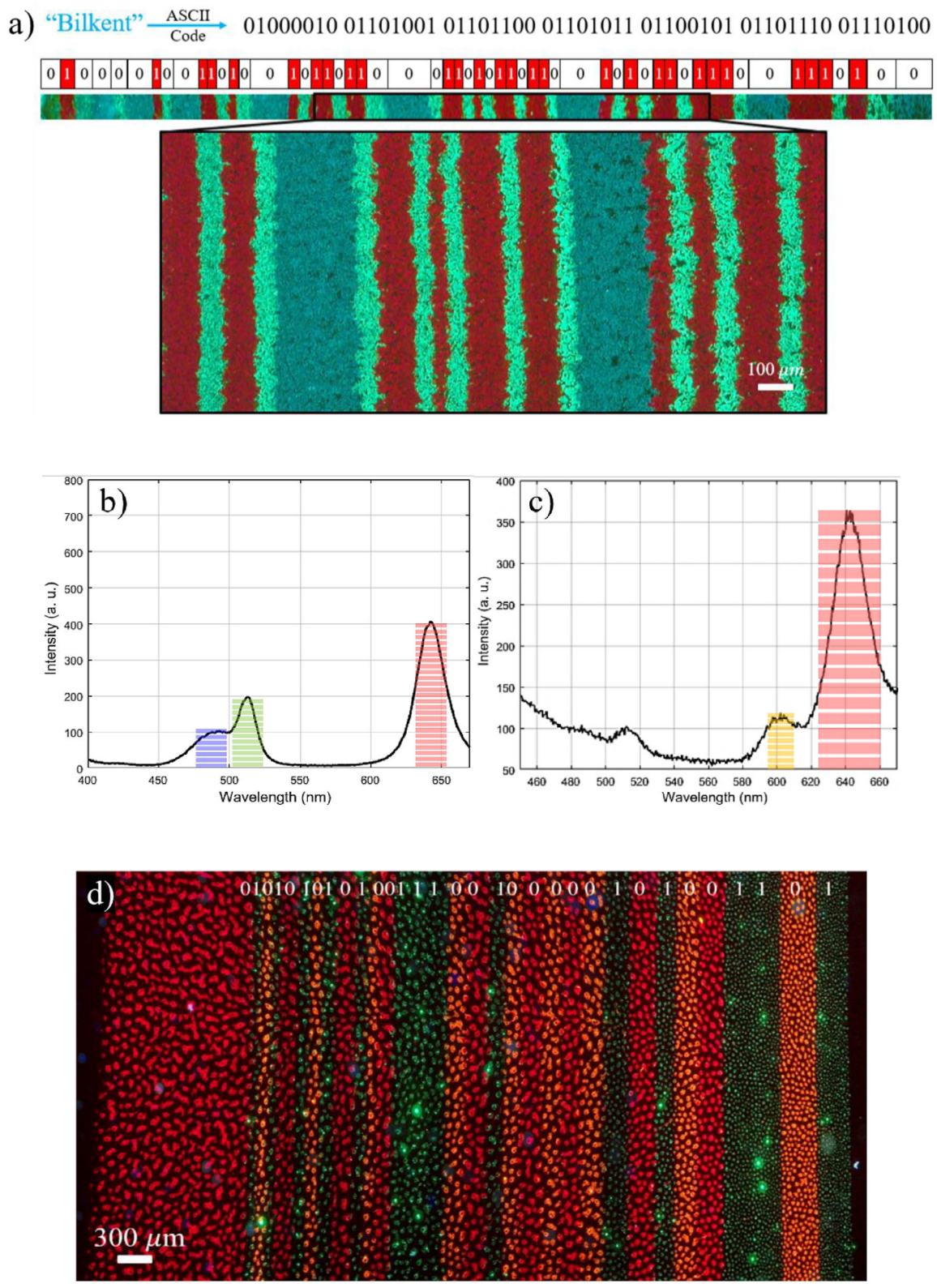

Figure 4. a) Fluorescent microscopy image of spatially encoded nanocrystal label corresponding to the word "Bilkent" in binary according to the ASCII code. The red strips represent 1, and the blue and green stripes represent 0. To emphasize the information, the label was cropped into a ribbon. b) PL response of the label under ultraviolet (UV) exposure representing the number "7577" corresponding to "0 101 0101 0 100 1110 0 100 0001 0 100 1101″ in binary. c) Optical response of the spatially and spectrally encoded label under UV exposure, representing the number "306" corresponding to "010 011 0010" in binary. d) Fluorescent microscopy image of spatially and spectrally encoded label representing the word "UNAM" corresponding to "0 101 0101 0 100 1110 0 100 0001 0 100 1101″ in binary.

utmost importance for later decoding and reading the label. The CQWs are not interfused with each other and possess a spatial resolution of micrometers, which is otherwise costly to achieve with conventional methods. This desirable resolution further enables encoding in microscale, rather than conventional miliscale, making it exceptionally appealing for microdevice labelling applications. Unlike normal barcodes that use just one color, with our method, multiple colors can be exploited to encode the information. Thus, multiple sets of information can be encoded. The encoding capacity (total number of cases) is calculated as $m \times (2^n - 1)$, in which n is the number of data bits (stripes), and m is the number of colors. CQWs, with their ultra-narrow emission bandwidth, provide a large m, leading to superior encoding capacity in the information-encoded nanocrystal labels.

2.3. Spectral Encoding

Besides spatial encoding, our method makes spectral encoding possible, which can add another level of complexity to the information. Here, the number and the color of the stripes are noteworthy since the emission spectrum is measured and used for encoding. Every word or number can be converted to binary and then a specific number of bits can be assigned to a color. Ultimately, those assigned bits of data for each color, are converted back to decimal to determine the number of stripes to fabricate the label. The spectral encoding as one layer of intricacy gives us a total of $(m + 1)^n - 1$ instances as encoding capacity. For example, to spectrally encode "7577", with the binary number "0 011 101 100 11001", 15 bits of data are needed in total. Encoding with three colors, each color will have 5 bits (00111:0 1100:11 001; blue: green: red), and thus, by converting each section from binary to decimal, we will need 7 blue, 12 green, and 25 red stripes (a total of 44 stripes). Figure 4b shows the PL spectrum of the label. To decode data from the spectrum and find the number of stripes, the area under each emission should be calculated and divided by the area under the curve of a single stripe. Since the number of stripes is an integer number, the integer part needs to be taken using the following equation:

$$n_{color} = \lfloor \frac{S_{color}}{S_{stripe}} \rfloor \quad (1)$$

in which n_{color} is the number of stripes related to the specific color, S_{color} is the area under each emission, and S_{stripe} is the area under the emission of a single stripe. The single stripe in the label has dimensions of 0.1 mm × 3.5 mm.

2.4. Opto-Spatial Encoding

A simultaneous spectral and spatial encoding is also possible by employing our method, which can boost the encoding capacity. Assuming m colors for encoding, $p = 1$ to $m - 1$ of the colors can be designated for spatial encoding, and other colors can be designated for spectral encoding. The encoding capacity of spatial encoding is $p \times (2^n - 1)$ and for spectral encoding is $(q + 1)^n - 1$, where p is the number of colors occupied for spatial coding, and $q = m - p$ is the number of colors occupied for spectral encoding. For example, to encode "UNAM 306" opto-spatially, "UNAM" is encoded spatially and "306" is encoded spectrally. As "UNAM" corresponds to "0 101 0101 0 100 1110 0 100 0001 0 100 1101" in ASCII code, taking green stripes as 1 and orange and red stripes as 0, 14 green stripes in the pattern are required. To spectrally encode "306", equivalent to "010 011 0010" in binary, two colors of orange and red are utilized, in which each color contains 5 bits of data (0 1001:10 010; orange: red). Hence, 9 orange stripes and 18 red stripes are desired. Figures 4c,d display the information-encoded label and its spectrum. Variant encoding schemes can also be considered to enhance the capacity and complexity of encoding (Figures S14–S16, Supporting Information).

To design and fabricate unclonable labels as PUFs, labels need to have an element of randomness. The required randomness is inherently fulfilled during the proposed fabrication process through the random spatial positioning of the fluorescent domains. CQWs generate randomly positioned microscale domains that form during the deposition and subsequent ring formation when silicone oil is added. This randomness is amplified by the edges introduced by the boundaries of the rings. The use of an excessive amount of silicone oil is crucial for pushing the rings and deforming them from straight lines to zigzag lines. In terms of randomness, we generated the randomness on the boundaries of stripes instead of the PL intensity of the materials that could undergo photobleaching. Otherwise, the usage time of the label on the product will be limited. This approach of using the randomness of the edges extends the lifetime of the PUF labels. Different combinations of CQWs, emitting at various wavelengths, were patterned periodically with a high level of randomness at the edges, which are shown in Figure S7 (Supporting Information). The randomness and PUF metrics of these self-assembled CQW labels were evaluated by the generation of binary keys. A computational procedure (see SI for details) was used to convert fluorescence microscopy images into 16×16 binary images. This computational procedure involves processing of the original images by converting them to grayscale, refinement via noise reduction and thresholding. The binary keys are finally subjected to the von Neumann debiasing algorithm, which effectively removes undesired repetitions.

Figure 5a presents a representative image and the corresponding binary image (see Figure S17, Supporting Information for other images). These binary keys were then applied to calculate commonly accepted PUF metrics. The equal distribution of 0-bits and 1-bits was measured with uniformity, where 0.5 is ideally expected. The uniformity (Figure 5b) was close to this ideal value with an arithmetic average of 0.4938. To further confirm the randomness of bitstreams, 7 different statistical tests were undertaken, which have been proposed by the National Institute of Standards and Technology (NIST).[49] Table S3 (Supporting Information) lists p-values and pass rates. The p-values were found to be greater than 0.01. Overall, the total sequence of 4352 bits generated from fluorescence microscopy images of these PUFs passed all 7 tests, confirming the randomness of the generated patterns. An additional metric that assesses the suitability for authentication is the uniqueness, which is calculated (see SI for details) by using inter-chip Hamming distance (HD_{INTER}).[50] The distribution of HD_{INTER} of these CQW PUFs was centered around 0.5 (Figure 5c). The uniqueness was calculated as 0.5060 ± 0.0323. The closeness of this value

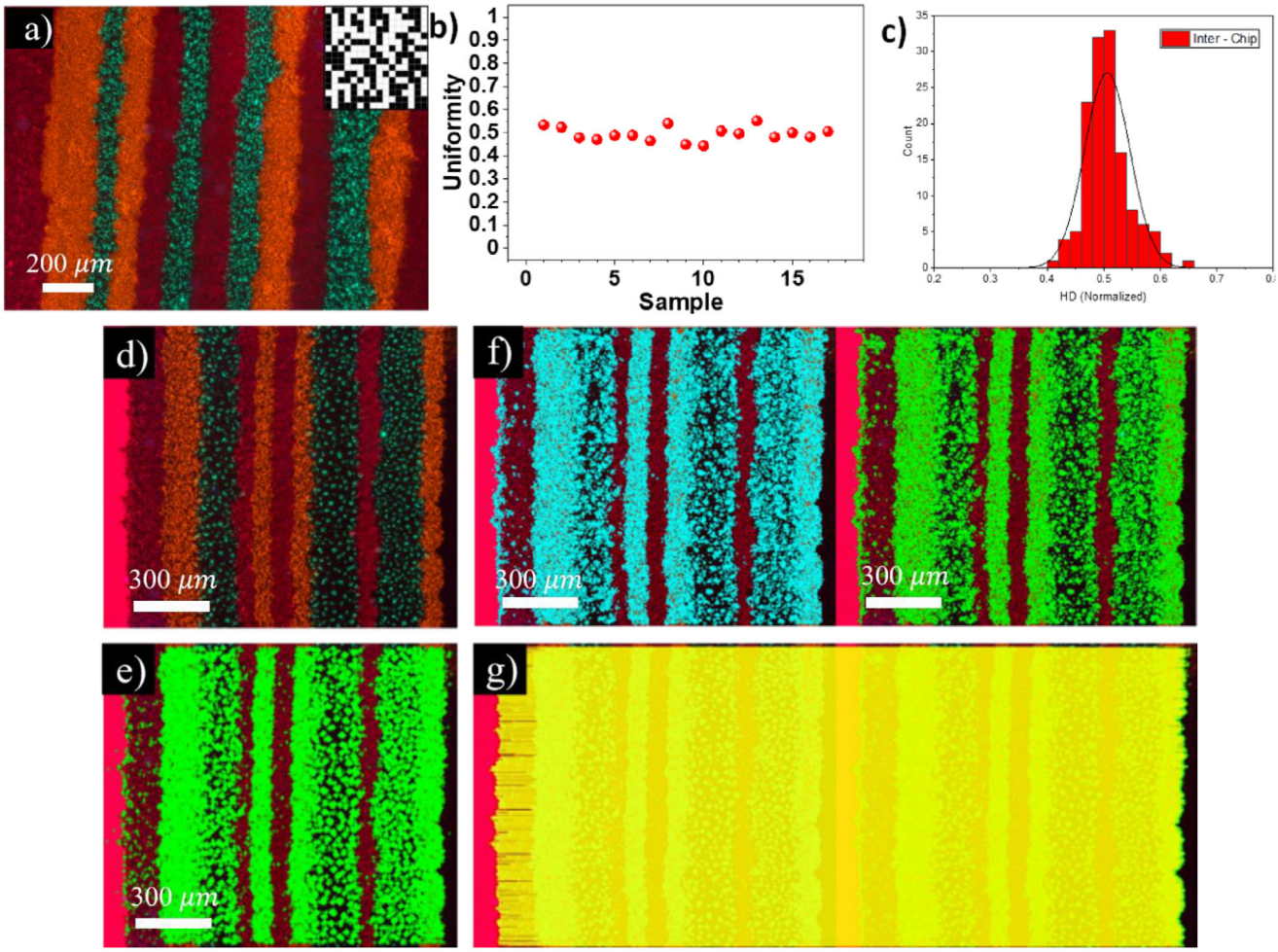

Figure 5. PUF performance and authentication using a feature matching algorithm. a) Representative fluorescence microscopy image. The inset (top right) shows the corresponding binary image. b) Inter-device Hamming distance. c) Uniformity of bits obtained from samples. d) Images used as keys. e) Identification of key points for each image. f) Image matching using the ORB algorithm. g) Connecting the matched points with a line.

to 0.5 is a good indication of the suitability of such keys for authentication.

In the authentication process, matching was performed by considering the imaging conditions and especially the constraints related to the spatial position of the image. In the first place, images were obtained, and a database was created. The images were manually rotated by 90° and 180° and added to the database. Then, using the ORB (oriented FAST and rotated BRIEF) algorithm, image features were extracted and compared with those stored in the database. Figures 5d–g provide examples of this image-matching process. Figure 5d shows the tag image used and Figure 5e depicts the key points extracted from this image. In this image, 135616 key points were detected by the ORB algorithm (Figure 5f). Lastly, the matching points were shown with yellow lines (Figure 5g). The ORB algorithm can match images captured at different rotation angles with a high accuracy of 99.27% at 90° and 99.70% at 180° (Figure S18, Supporting Information). This authentication scheme gives successful matching results of 89.58% even when only a partial region of the image was used (Figure S19, Supporting Information). These matching results are quite low for images that are not in the database (Figure S20, Supporting Information). The authentication process can be performed quickly and reliably with images from any location, regardless of scale, rotation, and other viewing conditions.

To be practically applicable in real-life applications, the information-encoded labels should be transferrable to various targets with different surface chemistries. In IoT applications, one of the main concerns in security is the chip validity. Several techniques can be employed to construct unclonable chips.[5] Most of these techniques are pricey due to CMOS node technology fabrication.[51] Therefore, we designed and fabricated an ultradurable cost-effective information-encoded anti-counterfeiting CQW label that can be attached to the exterior of the chips. To demonstrate the versatility of these labels and the possibility of their transfer, a 5×14 mm^2 information-encoded label was transferred onto a semiconductor chip using tattoo paper, as shown in **Figure 6**a. Figure 6b displays the location of the label under UV light, and Figure 6c depicts the fluorescent image of the transferred PUF label. Two colors are employed to display the information: green as 1 and red as 0, indicating the chip serial number as 111 011 001, in a spatially-encoded binary format. First,

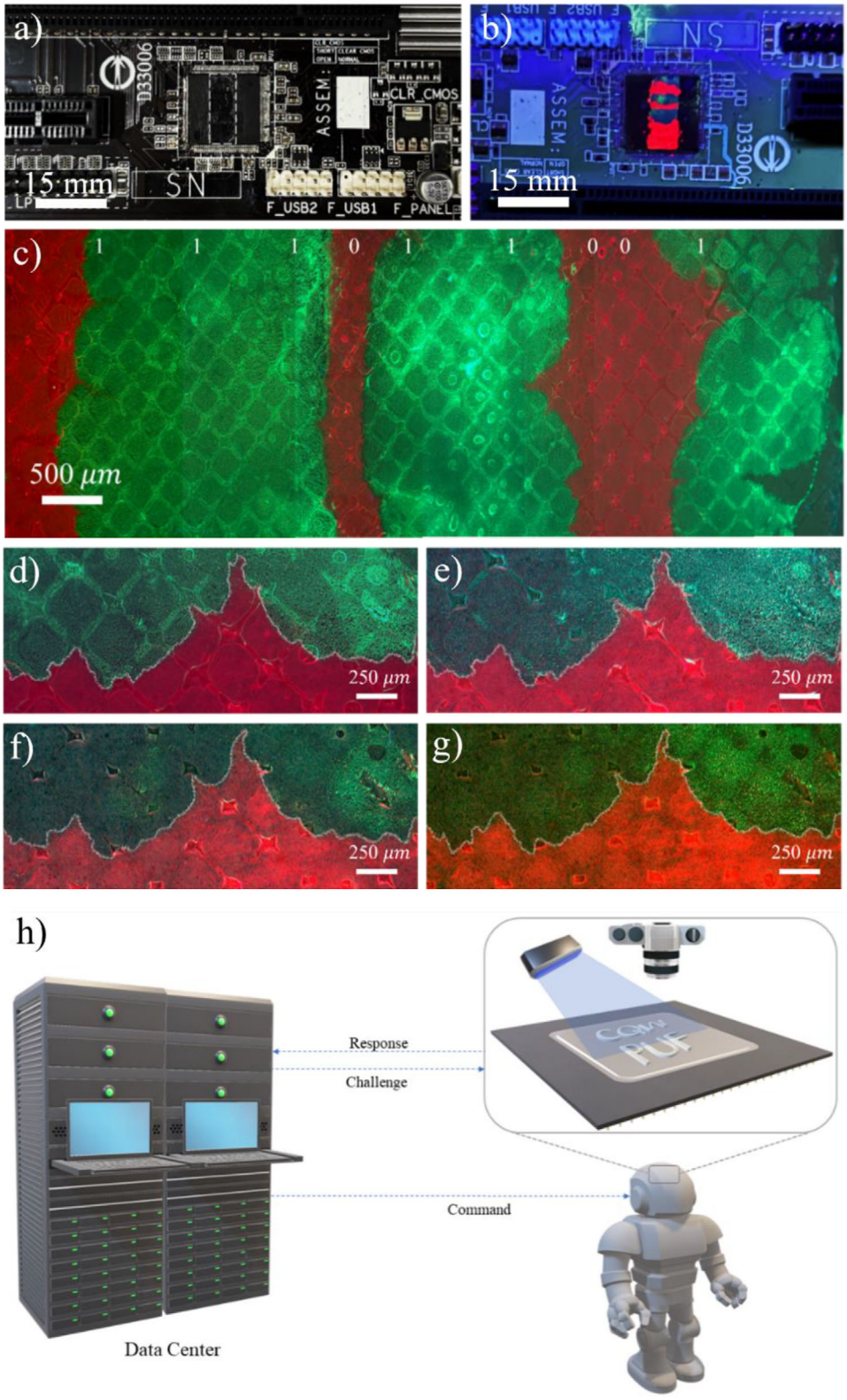

Figure 6. a) Our CQW PUF label on the chip under ambient light. b) The label on the chip under UV exposure. c) Demonstration of the label information under a fluorescent microscope with "111 011 001" information in binary. d) Boundary of two CQW stripes right after the labelling. e) Boundary of two CQW stripes 21 days after the labelling. f) Boundary of two CQW stripes after heating the chip at 100 °C for 1 hour. g) Boundary of two CQW stripes after 3 successive heating and putting the chip inside the water for 65 minutes. h) The protocol for information-encoded optical PUF usage in daily life. To turn the robot on, a request will be sent to the data center with the image of the label. After the label identity check, the system will be turned on by the data center if the image matches the database keys.

patterning was performed on the subphase and transferred to a tattoo paper, and then, the tattoo paper was transferred onto the chip using the stamping method. Figure 6h illustrates the protocol for validity check of the different instruments, including human robots in daily life. To prevent hardware attacks on the chips in IoT, our labels can be attached to the surface of the chips. Then, the information and the image of the PUF label will be read using a camera in the presence of UV light. The protocol begins with the validation of the chip, sending a challenge (optical) to the instrument to capture the label image. Then, the image will be sent to the data center to check its validity by comparing it with the security keys in the database. These PUFs can be authenticated using deep learning-based artificial intelligence (AI) algorithms to reduce the read-out time. After verification of the PUF, the instrument operates with the proper command from the data center.

Figure 6d shows the boundary of two stripes right after the labelling, highlighted with a white line. High-temperature, humidity and UV exposure tests were carried out to test the stability and durability of the label. To examine thermal stability, 21 days after labelling (Figure 6e), we heated the chip on a hot plate at 100 °C for 1 hour. No considerable change was observed (Figure 6f). This temperature is beyond the operation temperature range of the semiconductor chips, which is considered to be between 20 to 60 °C.[52] We repeated the same thermal stability test for three successive days. As a result, no significant change was observed (see Figure S21, Supporting Information), and the boundaries of the stripes remained unchanged. After the thermal stability test, to examine the stability of the label in the humidity condition, we submerged the chip inside a glass of water for 65 minutes. The fluorescent image demonstrates no considerable change (Figure 6g). Since the label could be read out several times after the labelling, we performed a UV stability test. The label was exposed to the UV light (10 mW) for 1 hour. Stability and durability tests were carried out continuously, and the captured images prove the high stability against high temperature, humidity, and UV exposure, and the 150-day durability of the label (Figure S21f, Supporting Information), confirming that the label is ultra durable. Figure S22 (Supporting Information) shows the stability and durability tests timeline. The stability test comparison between our labels and other labels in Table S4 (Supporting Information) indicates that our labels are among the ultra-durable ones reported thus far. Furthermore, we fabricated and exposed another label to ambient light for two weeks. There was no change in the boundaries of the stripes (Figure S23, Supporting Information), confirming the ultra-stability of the label. Then, another label was fabricated and put inside the three bottles of ethanol, hexane, and acetone, respectively, for one minute each. There was no change in the boundaries when the label was exposed to ethanol (Figure S24b, Supporting Information). In the case of hexane, a little change was observed in the boundaries of the stripes (Figure S24c, Supporting Information). Nonetheless, when the label was exposed to acetone, some alterations in the boundaries of the stripes (Figure S24d, Supporting Information) took place. However, labels are not suitable for long-time exposure to chemical solvents.

We made an approximate estimation of the label fabrication cost (Table S5, Supporting Information). The production cost of a 0.5 cm^2 label is estimated to be 6 cents, which puts our work among the cost-effective methods for anti-counterfeiting label manufacturing (Table S6, Supporting Information). Ultimately, the high-stability and low-cost scalable fabrication method of our CQW-PUF labels puts them among the most appealing candidates for large-scale commercialization. Furthermore, we compared the statistical test results of the labels in this work with those of previously reported labels in terms of uniqueness, randomness, and encoding capacity (Tables S7–S9, Supporting Information). For industrial applications, the high level of randomness and uniqueness, low manufacturing cost and high durability are among the most critical factors. To ensure industrial viability, the total cost of a PUF label should be minimized. In addition, as changing the obsolete labels of the products will be costly, the ultra-durability of the labels is a requirement in industrial applications. These PUF labels can be used, for example, on the surface of chips inside electronic devices. They can be further encapsulated with a specific protective layer if desired.

3. Conclusion

In this work, we proposed and fabricated cloneable and unclonable CQW labels with superior optical properties using a novel cost-effective method. Successive CQW macrodroplets were instilled to form rings on the subphase and then silicone oil was used to push the CQW rings and diminish their width into the desired pattern. Stamping was utilized to transfer a portion of the CQW rings to the target as an information-encoded label. Our CQW labels can be encoded spatially, spectrally, or both at the same time. To fabricate unclonable CQW labels, an excessive amount of silicone oil was used to compress the CQW rings intensely, causing deformation of the CQW ring boundaries. Since these CQW stripes have random edges within these labels, they cannot be replicated and are well-suited for anti-counterfeiting applications. Our results from the statistical tests alongside the uniqueness of 0.5060 ± 0.0323 proved the existence of randomness in our CQW PUFs, almost impossible to duplicate. Also, a feature-matching algorithm was used for the authentication of the CQW labels. An information-encoded label was transferred onto the surface of a semiconductor chip. The fabricated label exhibited 150-day durability and strong stability when exposed to high temperature and humidity. The high capacity of encoding due to the ultra-narrow emission bandwidth of the CQW, the cost-effectiveness of the proposed CQW labels and their high stability against high temperatures, humidity, and UV exposure make them unique and excellent candidates for commercialization in anti-counterfeiting applications. This study will open the way for the development of active anti-counterfeiting devices based on our CQW labels.

4. Experimental Section

Synthesis of 4 Monolayer (ML) CdSe and Alloyed $CdSe_{0.7}S_{0.3}$ Core CQWs: CdSe core CQWs were synthesized based on a published recipe of our group.[37] In a typical synthesis, 360 mg of cadmium myristate, 24 mg of Se, and 30 mL of ODE were mixed in a 100 mL three-neck RB flask, and the reaction mixture was vacuumed at 95 °C for 1 hour. Then, the flask was flushed with nitrogen gas, and the temperature was set to 240 °C. When the color of the solution turned golden yellow at temperatures around 195 °C, 120 mg of $Cd(OAc)_2 \cdot 2H_2O$ was swiftly added to the reaction solution

to initiate anisotropic growth of the CQWs. After 10 minutes of growth at 240 °C, 1 mL of OA was injected, while the flask was rapidly cooled down in a water bath. The solution was diluted with 10 mL of hexane and centrifuged to precipitate out the unstable species. Then, the CQWs were precipitated by the addition of ethanol and centrifugation at 6000 rpm for 6 minutes. The final CQWs were redispersed in hexane and used as seeds for the formation of the heterostructures. The synthesis procedure for 4 ML $CdSe_{0.7}S_{0.3}$ core CQWs is similar to CdSe CQWs, except that at 100 °C, 1 mL of S precursor (S-ODE, 0.2 M) was added to the solution.[47] The rest of the procedure is the same as the CdSe core CQWs recipe.

Synthesis of CdSe/CdS and $CdSe_{0.7}S_{0.3}$ /CdS Core/Crown CQWs: CdSe/CdS and $CdSe_{0.7}S_{0.3}$ /CdS core/crown CQWs were synthesized following a similar synthesis procedure adopted from the literature.[37] Briefly, 5 mL of ODE, 100 µL of OA, and 1 mL of 4 ML CdSe or CdSeS CQWs core solution (having an optical density of ≈1 at 350 nm when 100 µL of the core was dissolved in 3 mL of hexane) were mixed in a 50 mL three-neck RB flask and degassed at 90 °C for 30 minutes. Under argon flow, a mixture of 600 µL of Cd crown solution and 900 µL of S-ODE (0.1 M) was injected into the flask, and the temperature was set to 225 °C. When the temperature reached 225 °C, the flask was immediately quenched in a water bath. The solution was mixed with 5 mL of hexane and centrifuged at 6000 rpm for 6 minutes to remove unstable and unwanted species. Then, the CQWs were precipitated by the addition of ethanol and centrifugation. Finally, the core/crown CQWs were redispersed in hexane and kept for later use.

Synthesis of CdSe/CdZnS and CdSe/ZnS Core/Shell CQWs: CdSe/CdZnS core/shell CQWs were synthesized based on a reported recipe of our group.[53] Typically, 2 mL of the CdSe core solution in hexane (optical density of 1 at 350 nm, when 100 µL of the solution was added to 3 mL of hexane), 0.15 mmol of zinc acetate, 0.05 mmol of cadmium acetate, 0.5 mL of OA and 5 mL of ODE were mixed in a 50 mL three-neck RB flask. The mixture was degassed at 50 °C for 1 hour and further at 80 °C for 30 minutes. Then, the flask was flushed with nitrogen gas, the temperature was set to 300 °C, and 0.5 mL of OLA was injected into the flask. At temperatures around 155–160 °C, a sulfur precursor of 1-octanethiol in ODE (0.1 M) was started to be injected into the reaction solution with an initial injection rate of 10 mL h^{-1} for temperatures below 240 °C and later 4 mL h^{-1} for temperatures above 240 °C. The injection continued while aliquots were taken from the solution to track the emission peak wavelength. At the preferred emission peak wavelength, the injection was stopped, and the flask was quenched in a water bath. The CQWs were diluted with 5 mL of hexane, and the solution was centrifuged to remove the unstable species. The CQWs were precipitated from the solution by the addition of ethanol and centrifugation. Finally, the CQWs were redispersed in hexane for further use. CdSe/ZnS core/shell CQWs were synthesized following a similar recipe, except that no cadmium acetate was added to the flask and the amount of zinc acetate was increased to 0.2 mmol. The rest of the synthesis procedure was identical to CdSe/CdZnS core/shell CQWs.

Label Fabrication: A plastic Petri dish was used as the subphase container. Diethylene glycol was poured into the Petri dish to fill the Petri dish to the edge. 1 mL cc^{-1} sterile syringe was used for injecting the CQW solution on the subphase which was attached to a metal stand. A homemade metal rod was produced to be used in the stamping process. The substrate was attached to the back end of the rod.

Supporting Information

Supporting Information is available from the Wiley Online Library or from the author.

Acknowledgements

The authors acknowledge support from TUBITAK 2247-A National Leader Researchers Program (121C266) and H.V.D. gratefully acknowledges partial support from TUBA-Turkish Academy of Sciences.

Conflict of Interest

The authors declare no conflict of interest.

Data Availability Statement

The data that support the findings of this study are available from the corresponding author upon reasonable request.

Keywords

anti-counterfeiting labels, chip security, colloidal quantum wells, information-encoded labelling, physical unclonable functions, spatial encoding, spectral encoding

Received: September 2, 2025
Revised: November 1, 2025
Published online: November 28, 2025

[1] G. Yin, G. Huo, M. Qi, D. Liu, L. Li, J. Zhou, X. Le, Y. Wang, T. Chen, *Adv. Funct. Mater.* **2024**, *34*, 2310043.
[2] J. W. Leem, M. S. Kim, S. H. Choi, S.-R. Kim, S.-W. Kim, Y. M. Song, R. J. Young, Y. L. Kim, *Nat. Commun.* **2020**, *11*, 328.
[3] Y. Liu, F. Han, F. Li, Y. Zhao, M. Chen, Z. Xu, X. Zheng, H. Hu, J. Yao, T. Guo, W. Lin, Y. Zheng, B. You, P. Liu, Y. Li, L. Qian, *Nat. Commun.* **2019**, *10*, 2409.
[4] Y. Huo, Z. Yang, T. Wilson, C. Jiang, *Adv. Mater. Interfaces* **2022**, *9*, 2200201.
[5] K. Wang, J. Shi, W. Lai, Q. He, J. Xu, Z. Ni, X. Liu, X. Pi, D. Yang, *Nat. Commun.* **2024**, *15*, 3203.
[6] J. Zhang, R. Tan, Y. Liu, M. Albino, W. Zhang, M. M. Stevens, F. F. Loeffler, *Nat. Commun.* **2024**, *15*, 1040.
[7] Y. Sun, D. Lou, W. Liu, Z. Zheng, X. Chen, *Adv. Opt. Mater.* **2023**, *11*, 2201549.
[8] X. Fang, H. Ren, M. Gu, *Nat. Photonics* **2020**, *14*, 102.
[9] S. Shikha, T. Salafi, J. Cheng, Y. Zhang, *Chem. Soc. Rev.* **2017**, *46*, 7054.
[10] W. Ren, G. Lin, C. Clarke, J. Zhou, D. Jin, *Adv. Mater.* **2020**, *32*, 1901430.
[11] H. Im, J. Yoon, J. Choi, J. Kim, S. Baek, D. H. Park, W. Park, S. Kim, *Adv. Mater.* **2021**, *33*, 2102542.
[12] N. F. König, A. Al Ouahabi, L. Oswald, R. Szweda, L. Charles, J. F. Lutz, *Nat. Commun.* **2019**, *10*, 3774.
[13] N. B. Kiremitler, A. Esidir, G. A. Drake, A. F. Yazici, F. Sahin, I. Torun, M. Kalay, Y. Kelestemur, H. V. Demir, M. Shim, E. Mutlugun, M. S. Onses, *Adv. Opt. Mater.* **2024**, *12*, 2302464.
[14] M. Liebel, N. Pazos-Perez, N. F. van Hulst, R. A. Alvarez-Puebla, *Nat. Nanotechnol.* **2020**, *15*, 1005.
[15] J. Zhang, Y. Liu, C. Njel, S. Ronneberger, N. V. Tarakina, F. F. Loeffler, *Nat. Nanotechnol.* **2023**, *18*, 1027.
[16] Z. Zheng, H. Hu, Z. Zhang, B. Liu, M. Li, D.-H. Qu, H. Tian, W.-H. Zhu, B. L. Feringa, *Nat. Photonics* **2022**, *16*, 226.
[17] Y. Gao, S. F. Al-Sarawi, D. Abbott, *Nat. Electron.* **2020**, *3*, 81.
[18] R. Arppe, T. J. Sørensen, *Nat. Rev. Chem.* **2017**, *1*, 0031.
[19] J. Andres, R. D. Hersch, J.-E. Moser, A.-S. Chauvin, *Adv. Funct. Mater.* **2014**, *24*, 5029.
[20] P. Kumar, S. Singh, B. K. Gupta, *Nanoscale* **2016**, *8*, 14297.
[21] M. Han, X. Gao, J. Z. Su, S. Nie, *Nat. Biotechnol.* **2001**, *19*, 631.
[22] Z. Lu, Y. Liu, W. Hu, X. W. (D.) Lou, C. M. Li, *Chem. Commun.* **2011**, *47*, 9609.
[23] Z. Zeng, B. Huang, X. Wang, L. Lu, Q. Lu, M. Sun, T. Wu, T. Ma, J. Xu, Y. Xu, S. Wang, Y. Du, C.-H. Yan, *Adv. Mater.* **2020**, *32*, 2004506.

[24] Y. Cui, R. S. Hegde, I. Y. Phang, H. K. Lee, X. Y. Ling, *Nanoscale* **2014**, *6*, 282.
[25] D. Li, L. Tang, J. Wang, X. Liu, Y. Ying, *Adv. Opt. Mater.* **2016**, *4*, 1475.
[26] Kanika, G. Kedawat, S. Srivastava, B. K. Gupta, *Small* **2023**, *19*, 2206397.
[27] L. Kong, X. Zhang, C. Zhang, L. Wang, S. Wang, F. Cao, D. Zhao, A. L. Rogach, X. Yang, *Adv. Mater.* **2022**, *34*, 2205217.
[28] P. Mishra, A. Manna, N. Ray, *Nanoscale* **2025**, *17*, 20865.
[29] R. Guo, M. Zhang, J. Ding, A. Liu, F. Huang, M. Sheng, *J. Mater. Chem. C* **2022**, *10*, 7404.
[30] G. Almeida, L. van der Poll, W. H. Evers, E. Szoboszlai, S. J. W. Vonk, F. T. Rabouw, A. J. Houtepen, *Nano Lett.* **2023**, *23*, 8697.
[31] B. Cook, M. Gong, D. Ewing, M. Casper, A. Stramel, A. Elliot, J. Wu, *ACS Appl. Nano Mater.* **2019**, *2*, 3246.
[32] D. Yu, W. Zhu, A.-G. Shen, *Nanoscale Adv.* **2023**, *5*, 6365.
[33] L. Nayak, S. Mohanty, S. K. Nayak, A. Ramadoss, *J. Mater. Chem. C* **2019**, *7*, 8771.
[34] Z. Nie, E. Kumacheva, *Nat. Mater.* **2008**, *7*, 277.
[35] Q.i Zhang, Y. H. Lee, I. Y. Phang, C. K. Lee, X. Y. Ling, *Small* **2014**, *10*, 2703.
[36] O. Erdem, S. Foroutan, N. Gheshlaghi, B. Guzelturk, Y. Altintas, H. V. Demir, *Nano Lett.* **2020**, *20*, 6459.
[37] F. Shabani, H. Dehghanpour Baruj, I. Yurdakul, S. Delikanli, N. Gheshlaghi, F. Isik, B. Liu, Y. Altintas, B. Canimkurbey, H. V. Demir, *Small* **2022**, *18*, 2106115.
[38] J. Yu, S. Hu, H. Gao, S. Delikanli, B. Liu, J. J. Jasieniak, M. Sharma, H. V. Demir, *Nano Lett.* **2022**, *22*, 10224.
[39] H. L. Nguyen, T. N. Do, E. G. Durmusoglu, M. Izmir, R. Sarkar, S. Pal, O. V. Prezhdo, H. V. Demir, H.-S. Tan, *ACS Nano* **2023**, *17*, 2411.
[40] A. A. Rossinelli, H. Rojo, A. S. Mule, M. Aellen, A. Cocina, E. De Leo, R. Schäublin, D. J. Norris, *Chem. Mater.* **2019**, *31*, 9567.
[41] Y. Kelestemur, Y. Shynkarenko, M. Anni, S. Yakunin, M. L. De Giorgi, M. V. Kovalenko, *ACS Nano* **2019**, *13*, 13899.
[42] G. E. Bonacchini, C. Bossio, F. Greco, V. Mattoli, Y.-H.i Kim, G. Lanzani, M. Caironi, *Adv. Mater.* **2018**, *30*, 1706091.
[43] M. Riesner, F. Shabani, L. Zeylmans van Emmichoven, J. Klein, S. Delikanli, R. Fainblat, H. V. Demir, G. Bacher, *ACS Nano* **2024**, *18*, 24523.
[44] S. Delikanli, F. Isik, F. Shabani, H. D. Baruj, N. Taghipour, H. V. Demir, *Adv. Opt. Mater.* **2021**, *9*, 2002220.
[45] F. Isik, S. Delikanli, E. G. Durmusoglu, A. T. Isik, F. Shabani, H. D. Baruj, H. V. Demir, *Small* **2024**, *20*, 2309494.
[46] S. Hu, F. Shabani, B. Liu, L. Zhang, M. Guo, G. Lu, Z. Zhou, J. Wang, J. C. Huang, Y. Min, Q. Xue, H. V. Demir, C. Liu, *ACS Nano* **2022**, *16*, 10840.
[47] Y. Altintas, B. Liu, P. L. Hernández-Martínez, N. Gheshlaghi, F. Shabani, M. Sharma, L. Wang, H. Sun, E. Mutlugun, H. V. Demir, *Chem. Mater.* **2020**, *32*, 7874.
[48] O. Erdem, K. Gungor, B. Guzelturk, I. Tanriover, M. Sak, M. Olutas, D. Dede, Y. Kelestemur, H. V. Demir, *Nano Lett.* **2019**, *19*, 4297.
[49] L. E. Bassham III, A. L. Rukhin, J. Soto, J. R. Nechvatal, M. E. Smid, E. B. Barker, S. D. Leigh, M. Levenson, M. Vangel, D. L. Banks, N. A. Heckert, J. F. Dray, S. Vo, *SP 800-22 Rev. 1a. A Statistical Test Suite for Random and Pseudorandom Number Generators for Cryptographic Applications*, National Institute of Standards & Technology, Gaithersburg, MD, United States **2010**.
[50] N. Torun, I. Torun, M. Sakir, M. Kalay, M. S. Onses, *ACS Appl. Mater. Interfaces* **2021**, *13*, 11247.
[51] B. Park, D. Forte, M. M. Tehranipoor, N. Maghari, *IEEE Trans. Circuits Syst. I: Regular Papers* **2021**, *68*, 4700.
[52] M. D. Li, X. Q. Shen, X. Chen, J. M. Gan, F. Wang, J. Li, X. L. Wang, Q. D. Shen, *Nat. Commun.* **2022**, *13*, 5849.
[53] F. Shabani, M. Ahmad, S. Kumar, S. Delikanli, F. Isik, A. Bhattacharya, A. Petrou, H. V. Demir, *Chem. Mater.* **2023**, *35*, 4159.